Structure Changes in Model Membranes Monitored by Variable Period X-ray Standing Waves: Effect of Langmuir−Blodgett Film Thickness on Thermal Behavior

Jin Wang and Martin Caffrey*

Department of Chemistry, The Ohio State University, Columbus, Ohio 43210

Michael J. Bedzyk

Department of Material Science and Engineering, Northwestern University, Evanston, Illinois 60208, and MSD, Argonne National Laboratory, Argonne, Illinois 60439

Thomas L. Penner

Corporate Research Laboratories, Eastman Kodak Company, Rochester, New York 14650

Received: June 7, 1994®

Variable period X-ray standing wave (XSW) measurements have been used previously to monitor and to interpret structure rearrangements undergone during a phase transition in a model membrane with angstrom resolution. In the present study, an extended length scale ranging from 40 up to ca. 1000 Å has been used without sacrificing resolution to address the question of whether the phase transition characteristics of a lipid multilayer are sensitive to the number and identity of the lamellae in the membrane stack. The system chosen for examination consisted of an octadecanethiol (ODT) coated gold mirror on top of which a variable number (0, 2, 8, and 16) of ω-tricosenoic acid (C23, ωTA) bilayers followed by a single upper inverted bilayer of zinc arachidate (C20, ZnA) was deposited by the Langmuir−Blodgett (LB) technique. Variable period XSW measurements provided precise information on the zinc layer mean position and width and were used to track the collapse of the heavy atom layer during the thermotropic phase transition. Samples with and without the ωTA layers showed disparate pretransitional rearrangements, transition temperatures, and apparent cooperativity as well as final high-temperature zinc distribution. At sufficiently high temperatures, the ODT monolayer appears to desorb from the gold mirror surface to be replaced by a layer of zinc. In all samples containing ωTA, the cooperative transition occurred at ca. 72 °C, which has been shown by simultaneous calorimetry and low- and wide-angle time-resolved X-ray diffraction to correspond to the onset of melting of bulk ωTA. Thus, the remarkable result that *bulk behavior is displayed by as few as two LB bilayers of ωTA.* With all thin film samples, the temperature-induced structure change was not reversed upon cooling to and subsequent storage at room temperature.

Introduction

Interest in Langmuir−Blodgett (LB) films has grown significantly in recent years due to their current or potential application in microelectronics, nonlinear optics, and biosensing devices.[1] Further, LB films have been used successfully as models for biological membranes.[2] Accordingly, a systematic study of LB film structure and stability is essential if we are to understand their functional properties.[3] For an ultrathin film consisting of a limited number of LB monolayers (hereafter referred to as paucilamellar LB films), the nature of the film itself and its components, the substrate surface and the interface between layers, has a major bearing on the behavior of the film as a whole.[3−5] Fortunately, this kind of ultrathin film is particularly well suited for examining questions concerning the relationship between molecular structure and the thermal and other physicochemical properties in low-dimensional systems.

A variety of methods have been used to study LB films including neutron, electron, and X-ray diffraction and reflectivity measurements,[6−10] fluorescence[11] and Fourier transform infrared spectroscopy,[12−14] and Raman and surface plasmon scattering.[15] Surface analytical techniques such as X-ray photoelectron spectroscopy[16] and secondary-ion mass spectroscopy[17] have also been used. More recently, atomic force microscopy (AFM) has been implemented in examining the in-plane structure of an LB film in a very direct way.[3,18] Much of the work reported in the literature has been carried out on LB films with a large number of layers, which makes their analysis much less demanding. The difficulties encountered in studying paucilamellar LB films arise because of the limited amount of material interrogated during measurement and the corresponding weak signal from such systems.

In the past few years, long period X-ray standing wave (XSW) measurements have been developed and implemented for characterizing paucilamellar and multilamellar LB films.[19−22] Long period XSW generated by Bragg diffraction from a layered synthetic microstructure (LSM)[20] and by total external reflection from a mirror[21] were used to locate zinc and cadmium layers embedded in LB films incorporating zinc and cadmium arachidate (ZnA and CdA) with an accuracy of better than 0.3 and 2 Å, respectively.[20,21] Additionally, the thermal stability and thermotropic properties of the LB films were studied by measuring zinc and cadmium distribution in the films upon heating. Such measurements represent the first of a kind in which the temperature dependence of the structure of an LB film was investigated by tracing selectively the distribution of a single atom layer which served as a marked layer in the film and an indicator of film structural integrity.

In this article, we report on the structure and thermotropic properties of a series of heavy atom labeled paucilamellar LB films studied by using a variable period XSW formed upon a

® Abstract published in *Advance ACS Abstracts,* September 15, 1994.

0022-3654/94/2098-10957$04.50/0

gold mirror. The films were deposited on hydrophobic hydrocarbon-derivatized gold mirrors and had the following composition: (1) a single inverted ZnA bilayer (sample 1) and (2) an inverted ZnA bilayer atop 2, 8, and 16 ωTA bilayers (samples 2, 3, and 4, respectively). These samples have been used to address a series of questions regarding thin film thermal behavior as follows. How does LB film composition affect the structure and thermotropic properties of the adlayer? Are the thermally-induced structural transformations in these paucilamellar films reversible? Does the ωTA in these LB films behave differently in bulk as compared to thin film form? In the course of answering these questions, we demonstrate the profound sensitivity of variable period XSW to structural changes in paucilamellar films and the general utility of this method for characterizing thin films and model membrane systems.

Methods

Theoretical Background. As with other forms of light, two coherent X-ray plane waves can create an XSW field in the region where they overlap. The original XSW method developed in the 1960s[23-28] used dynamic Bragg diffraction from perfect single crystals. Here, the period of the XSW field is in the 1−4 Å range and is determined by the d-spacing of the crystal upon which the XSW is generated. Limited by such a small period and the associated modulo-d ambiguity, the conventional XSW method is effective in measuring positions of atoms at the surface of and within a crystal with a length scale comparable to a single bond length. Obviously, an XSW with a much longer periodicity is required if it is to be applied to the measurement of biologically relevant membrane systems composed of lipids and proteins having dimensions ranging from tens to hundreds of angstroms. Recently, two new XSW techniques were developed with such an application in mind. In the first technique, LSMs which are fabricated crystals with d-spacings available in the 20−100 Å range were used to generate the XSW field.[20] Accordingly, the XSW produced during Bragg diffraction has a period of 20−100 Å as dictated by the d-spacing of the LSM. The second so-called variable period XSW method is based on the total external or specular reflection of an X-ray plane wave from an X-ray mirror.[20,21,29] The period of the XSW varies from infinity to tens of angstroms depending on the incident angle and energy of the X-rays. We have shown that the XSW field is well-defined at close to 1000 Å above a mirror surface and that the position of a heavy atom layer in that distance range can be determined by the variable period XSW method with an accuracy of several angstroms.[29]

Since the index of refraction, n, for X-rays in most materials is less than unity, an X-ray beam striking a vacuum/mirror interface will be reflected totally when the incident angle, θ, is below the critical angle, θ_c. The index of refraction can be described as

$$n = 1 - \delta - i\beta \qquad (1)$$

where δ and β refer, respectively, to the refractive index decrement and the absorption index of the X-rays in the medium and are small quantities of magnitude $<10^{-5}$. Using Snell's law it can be shown that θ_c equals $(2\delta)^{1/2}$, which is in the range of several milliradians (mrad, 1 mrad = 0.057°) for most materials and X-ray energies. The standing wave generated by the interference of the coherently related incident and reflected plane waves has an associated period, D, the distance between two adjacent nodes or antinodes (more generally, the distance between two adjacent points with identical phase), at a given incident angle θ, of $\lambda/(2 \sin \theta)$, where λ is the X-ray wavelength. The period of the XSW at θ_c is referred to as the critical period

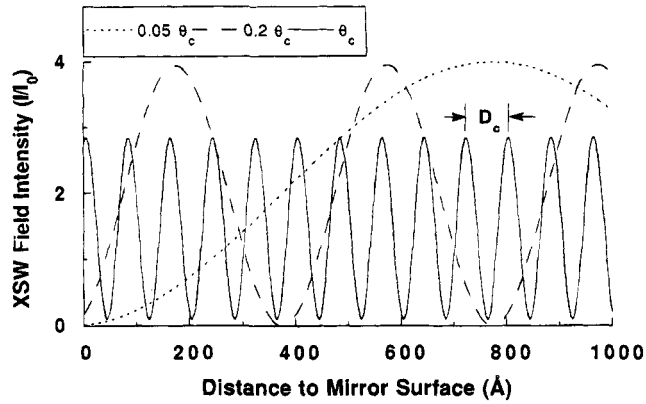

Figure 1. Spatial distribution of the normalized XSW E-field intensity at three different incident angles generated during specular reflection above the surface of a gold mirror. At an incident X-ray photon energy of 9.8 keV, the critical angle (θ_c) of the gold mirror is 7.85 mrad (0.449°). The critical period, D_c, indicated in the figure, is ca. 80 Å. The E-field intensities (I/I_0) are profiled at $0.05\theta_c$ (0.4 mrad, 0.023°), $0.2\theta_c$ (1.57 mrad, 0.09°), and θ_c (7.85 mrad). At low angles, the first antinode of the standing wave is quite distant from the surface and is next to the surface at the critical angle.

D_c ($= \lambda/(2 \sin \theta_c)$). For all practical purposes D_c is independent of photon energy because θ_c is approximately proportional to λ.[21,30]

The angular and positional, z, dependence of the XSW electric field (E-field) intensity in a vacuum above a mirror surface can be expressed as[21,31]

$$I(\theta,z) = I_0\left[1 + R + 2\sqrt{R}\cos\left(\nu - 2\pi\frac{z}{D}\right)\right] \qquad (2)$$

where I_0 is the intensity of the incident X-rays, R is the reflectivity of the X-ray mirror surface, and ν is the phase shift of the reflected plane wave at the surface. Shown in Figure 1 is a series of XSW E-field intensity profiles above a gold mirror surface at different incident angles. The calculations used in generating these profiles assume that the incident X-ray photon energy, E, is 9.8 keV, that the mirror is *in vacuo*, and that the refractive index, n, of the gold mirror is the same as gold in bulk form ($\delta = 3.08 \times 10^{-5}$, $\beta = 2.27 \times 10^{-6}$; see eq 1). At this photon energy, the critical angle of the gold mirror *in vacuo* is 7.85 mrad while the critical period is ca. 80 Å.

Referring to Figure 1, the angular dependence of the spatial distribution of the E-field intensity can be described as follows. For an incident angle close to zero, a node (minimum) is located at the mirror surface as a result of destructive interference between the incident and reflected X-rays while the first antinode (maximum) is at infinity. As the incident angle increases, the interference condition at the mirror surface becomes less destructive and the XSW period is reduced to finite size so that the first antinode moves toward the mirror surface. At the critical angle, the incident and reflected waves are in phase and interfere constructively. Thus, the first antinode becomes coincident with the mirror surface. The overall effect of increasing θ is to cause the XSW E-field to sweep inward toward the mirror surface like a collapsing bellows. The photoelectric effect which can be visualized as X-ray fluorescence is proportional to the E-field intensity sensed at the center of an atom. Thus, the fluorescence yield, Y, from a given *heavy* atom distribution $\varrho(z)$ in an XSW E-field of intensity $I(\theta,z)$ is

$$Y(\theta) = \int I(\theta,z)\,\varrho(z)\,dz \qquad (3)$$

In this application, we emphasize heavy atoms (large atomic numbers, Z) because of the ease with which the XSW

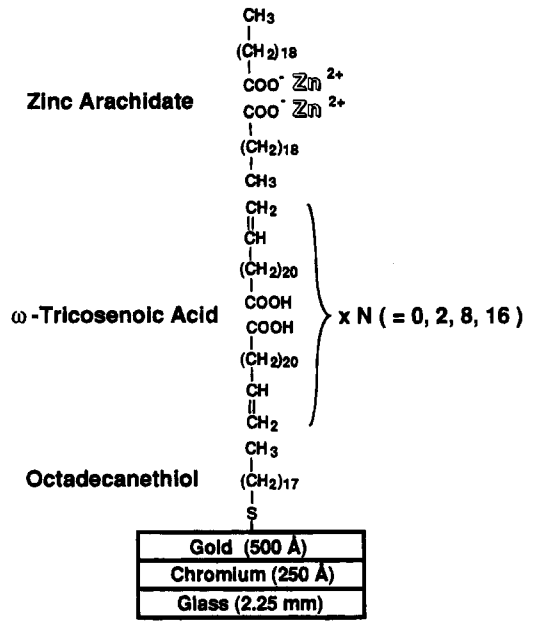

Figure 2. Schematic of the gold mirror and deposited films. Gold was deposited as a 500 Å thick film on a piece of chromium-coated float glass (5 cm × 2.5 cm × 0.2 cm) using thermoevaporation techniques. Before depositing the LB multilayers of ωTA and ZnA, the plasma cleaned gold surface was rendered hydrophobic with a self-assembled ODT monolayer. The sample numbers used in the text refer to the following: sample 1, $N = 0$ (no ωTA); sample 2, 3, and 4, $N =$ 2, 8 and 16, respectively. The dimensions shown for the mirror were obtained from the manufacturer's specifications.

fluorescence measurements can be performed with such materials. Thus, in a measurement where θ is varied, a fluorescence maximum is registered when an antinode of the XSW E-field coincides with the center of a heavy atom layer positioned above the mirror surface. Correspondingly, a minimum in the fluorescence yield profile is observed when an XSW node is coincident with the marker layer. Given that $I(\theta,z)$ can be calculated exactly, the position of a heavy atom layer above the mirror surface can be located unambiguously by deconvoluting the heavy atom distribution $\varrho(z)$ from the corresponding fluorescence yield profile. Further, the position of a heavy atom layer can be estimated rougly by counting the number of peaks in a fluorescence yield profile below θ_c. Thus, a profile with X peaks below θ_c has a heavy atom layer situated at $(X - 0.5)D_c$ above the mirror surface.

Sample Preparation. The structure and composition of the paucilamellar LB films and mirror used in this study are shown in Figure 2. Samples 1 and 2 were prepared at the Corporate Research Laboratories of the Eastman Kodak Company. Chemicals used in preparing these samples were of the highest purity available and were obtained from Eastman Kodak Co. (Rochester, NY) with the exception of $ZnCl_2$ which was purchased from Aldrich (Milwaukee, WI). The other samples (samples 3 and 4) were prepared at The Ohio State University for which all of the chemicals were purchased from Aldrich with the exception of arachidic acid which was obtained from Nu Chek Prep (Elysian, MN). Gold mirrors (Liberty Mirrors, Brackenridge, PA) were used as X-ray reflecting surfaces and as solid substrates for the LB films. The gold and chromium films in the mirror were thermally evaporated onto float glass slides with gold as the top layer. Mirrors were plasma cleaned (Model PDC-3XG, Harrick Scientific Corp., Ossining, NY; argon pressure, < 1.0 torr; high power setting) for 5 min to expose a fresh gold surface before being coated with organic films. Immediately upon removal from the plasma cleaner, the mirror was immersed in 1 mM ODT in tetrahydrofuran (THF) and incubated at room temperature for 6−12 h. The mirrors were rinsed extensively with THF to remove excess ODT. The thickness of the chemically bonded ODT monolayer was measured by ellipsometry (Model L116C, Gaertner Scientific Corp., Chicago, IL). Further, the advancing contact angle of a water droplet on the surface was monitored using a goniometer scope (Model 100-04, Ramé-Hart Inc., Mountain Lakes, NJ) by way of characterizing the hydrophobic surface. The contact angle was usually greater than 105° after ODT treatment indicating an extremely hydrophobic surface.[32]

LB film deposition was performed using either a KSV-2200 LB trough system (KSV Instruments, Riverside, CT) housed in a clean room at 23−25 °C in the Kodak lab or a KSV MiniTrough system (KSV Instrument) in an open lab with both temperature and relative humidity control at The Ohio State University. To begin with, 1 mM ωTA in chloroform was placed dropwise on an aqueous subphase consisting of freshly prepared Milli-Q water (Millipore Corp., Bedford, MA). The solvent was allowed to evaporate for at least 5 min before the film was compressed. In the first cycle of downstrokes and upstrokes, the deposition rate was 3.0 mm/min. The deposition rate was increased to 5.0 mm/min during additional cycles. All depositions were made at a surface pressure of 30 mN/m under feedback control where the area per ωTA molecule at the surface is 20 Å^2 based on the corresponding lateral pressure vs area/molecule isotherm. In preparation for depositing LB films of ZnA, a subphase containing 0.1 mM $ZnCl_2$ in 1 mM $NaHCO_3$ buffer (pH 7.1) was used. After the arachidic acid was spread from a 1 mM solution in chloroform as above and compressed, a ZnA monolayer formed at the air/subphase interface as a result of the electrostatic binding of Zn^{2+} to two arachidate carboxylate anions. The ZnA adlayers were prepared at a deposition rate of 3.0 mm/min and a surface pressure of 30 mN/m corresponding to an area of 40 Å^2 per ZnA. In the course of LB film deposition, monolayer transfer ratios were measured by monitoring the area loss of the film at the air/subphase interface per unit of substrate area passing through the interface. A transfer ratio of unity (±10%) was observed for all depositions. In the case of films prepared at the Kodak lab, ellipsometry was used to measure the thickness of successive layers immediately after each deposition segment was completed. Film thickness so determined was used in evaluating deposition quality. Following film preparation, samples were stored at room temperature in air. We have found that multilayers consisting of ωTA and ZnA deposited and stored as described above are stable for more than 3 years with no obvious structure deterioration.[33]

X-ray Standing Wave Measurements. The X-ray standing wave measurements were carried out in two separate experimental periods on the D-line at the Cornell High Energy Synchrotron Source (CHESS). Samples 1 and 2 were measured in the first and samples 3 and 4 in the second period. The Cornell electron−positron storage ring (CESR) was operated at 5.3 GeV and 30−50 mA or 60−100 mA total positron current, respectively, during the two running periods. The experimental arrangement used for making the XSW measurements has been described previously.[21,29,34] Polychromatic X-rays from the storage ring were monochromatized to 9.8 keV using a pair of flat germanium(111) crystals to optimally excite zinc K-fluorescence. The monochromator had an energy resolution of ca. 5 eV at 9.8 keV and a vertical divergence of less than 0.1 mrad (5.7 millidegrees).[34] The monochromated beam was collimated to between 20 and 40 μm in height and 2 mm in width by an $X-Y$ slit (Model 3013, Huber Diffraktionstechnik GMBH, Rimsting, Germany) after which the beam intensity was measured by using a 7.6 cm long, air-filled

ionization chamber. The typical incident X-ray intensity at the sample surface under the above experimental conditions was 10^7-10^8 photons/s.

X-ray fluorescence from the sample was acquired by using an energy-dispersive solid state Si(Li) detector (Model LS-33, Princeton Gamma-Tech, Princeton, NJ) with a measured energy resolution of 180 eV at 5.9 keV. The snout of the detector was positioned perpendicular to and in the same horizontal plane as the incident beam to reduce the contribution from scattered X-rays. The signal pulses from the detector were then amplified by a spectroscopy amplifier (Model TC 244, Tennelec, Oak Ridge, TN). Detector dead time correction was implemented by using a standard pulser from a random pulse generator (Model DB-2, Berkeley Nucleonics Corp., Berkeley, CA) positioned close (in energy) to the fluorescence signal of interest and with a similar count rate. A histogram memory module (Model 3588, LeCroy USA, Chestnut Ridge, NY) combined with a buffered analog-to-digital converter (ADC) unit (Model 3512, LeCroy USA) was used as a multichannel analyzer to record the entire fluorescence spectrum up to ca. 11 keV at each incident angle.

Sample reflectivity was recorded simultaneously with the fluorescence measurement and was calculated as the ratio of the incident and reflected beam intensities. For this purpose, two air-filled ionization chambers were positioned before (upstream) and after (downstream) the sample. A half-slit (Model 3013, Huber Diffraktionstechnik GMBH) was placed between the sample and the downstream ionization chamber in order to block the direct incident beam which passes over the sample at very low angles. When the sample was aligned parallel to the plane of the incident beam, i.e., at $\theta = 0°$, the upper surface of the slit was ca. 150 μm above the surface of the sample.

The sample was placed on a temperature regulated hot stage contained in an aluminum box with Kapton (0.001 in. thick, XTO Inc., Johnson City, NY) windows under a slight positive pressure of helium. The hot stage consisted of a power resistor (500 Ω, 30 W) attached to an aluminum block with a mass of ca. 80 g. A thin layer of thermal compound (Model 120−2, Wakefield Engineering Inc., Wakefield, MA) was applied to the contact area between the sample and the aluminum block. A thermocouple (chromel−alumel, type K, diameter 0.015 in., Omega Engineering, Inc., Stamford, CT), in contact with both the aluminum block and the under side of the sample, was used to record sample temperature. The hot stage temperature was regulated by a programmable temperature controller (Model 812, Eurotherm Corp., Reston, VA) with feedback control circuits. Temperature overshoot upon adjusting the temperature setting was limited to 1 °C throughout the experiment. The temperature variation over a period of 2 h at a preset temperature of 70 °C was no greater than ±1 °C. The helium box assembly was mounted on a goniometer head (Model 1003, Huber Diffraktionstechnik GMBH) attached to a Huber 410 goniometer (Huber Diffraktionstechnik GMBH). A careful alignment of the vertical setting of the goniometer head was made to ensure that the rotation axis of the Huber stage was coincident with the surface of the sample. With the sample in the horizontal position below the beam, its height was increased to the point where the incident beam intensity was exactly halved. Following this alignment procedure the center of the beam footprint on the sample remained fixed and coincident with the center of the sample and the rotation axis for all θ values. Under these conditions, a detector-to-footprint distance of 34 mm was observed.

The XSW measurements were made in the temperature range from 32 or 29 °C [room temperature (RT) in the D-line radiation hutch during the two experimental running periods, respectively] to 129 °C with the exception of sample 2 which was heated to 82 °C. For each sample, the measurement was performed in two stages. In the first stage, an identical duplicate sample was used in rapid (<1 s per angular step) zinc fluorescence yield measurements every 5 °C while the sample was subjected to a slow temperature ramping (<2 °C/min). In this way, the temperature range in which the phase transition occurred could be determined roughly. Then, the XSW measurement was repeated on a fresh sample under thermal equilibrium conditions with longer counting times to secure better counting statistics. Close to the phase transition, a temperature increment of 1 or 2 °C was used. Samples were allowed to equilibrate thermally at each new temperature setting for at least 10 min before making the XSW measurement. A temperature gradient of ca. 0.2 °C/mm existed across the width of the sample such that the temperature range across the 2 mm illuminated strip was <0.5 °C along the rotation axis of the sample. At each temperature, reflectivity and fluorescence data were collected in appropriate angular increments to ensure that enough data points were recorded to define each fluorescence peak. With the above experimental arrangement and a total positron current of 35−80 mA, counting times of 7−20 s were needed to accumulate zinc fluorescence data with 2% counting statistics below the critical angle. Thus, a θ scan consisting of 64 angular steps required from 8 to 22 min to complete.

Simultaneous Calorimetry and Time-Resolved X-Ray Diffraction. The simultaneous calorimetry and time-resolved X-ray diffraction (SCALTRD) method has been used previously to establish unequivocally the correlation of structure changes and thermal events in hydrated lipid systems.[35] In this study, the SCALTRD technique was used for the same purpose with bulk powdered ωTA.

Measurements were performed with a home-built calorimeter consisting of an X-ray transparent sample cell.[36] Both low- and wide-angle diffraction patterns were recorded in the form of a streak film[37,38] with a line X-ray source at 8.04 keV ($\lambda = 1.54$ Å, Cu target) from a Rigaku RU300 X-ray Generator (Rigaku/USA Inc., Danvers, MA) operated at 54 kV and 254 mA. The streak camera device incorporates a vertical slit (3 mm wide) behind which a film cassette is translated at a constant speed. The incident X-ray beam was focused at the film plane by a nickel coated, curved glass mirror (Charles Supper, Natich, MA). The sample-to-film distance was 18.08 cm. The temperature scan from 60 to 90 °C lasted ca. 9.5 h (3.2 °C/h) while the X-ray sensitive film (DEF5, Eastman Kodak Co., Rochester, NY) was translated at a rate of 10.8 mm/h. The calorimetric data have not been corrected for scan rate. However, the scan has been corrected for a linear baseline outside the transition region (T < 65 °C and T > 75 °C). The total amount of ωTA used in the SCALTRD measurement was 6.8 mg.

To obtain the transition enthalpy, heating and cooling scans of powdered ωTA (0.45 mg, molar mass 352.60 g) were measured with a calibrated, high-sensitivity differential scanning calorimeter (DSC, Hart Scientific, Pleasant Grove, UT) in the range 30−90 °C. Heating and cooling rates used were 0.5 °C/min. With the DSC data (heat capacity, C_p, as a function of sample temperature, corrected for scan rate), the transition enthalpy was calculated in two steps. First, the scans were corrected for a polynomial (order ≤ 5) baseline outside the transition region (T < 65 °C and T > 75 °C). Then, the area under the calorimetric peaks (65 < T < 75 °C) was calculated by a numeric computation package (Kaleidagraph, Abelback software, Reading, PA). Normalized by the number of moles of ωTA (1.27 μmol), this area value gives the transition enthalpy.

XSW Data Analysis. As noted above, the entire fluorescence spectrum was available for data analysis when the ADC/histogram memory modules were used in data collection. The Zn Kα peak at 8.6 keV was well resolved from scattered X-rays centered at 9.8 keV and from other fluorescence peaks in the spectrum. An accurate measure of total fluorescence counts was made by determining the area beneath the Zn Kα peak using a χ^2-fitting program. The integrated fluorescence intensity data extracted from the spectrum was then corrected for detector dead time by a live-time factor which is the ratio of the pulser counts recorded in the spectrum and the input pulser counts. This correction is needed because of the finite response time of the detector and the amplifier such that a part of the incident events (standard pulser and fluorescence photons) go unamplified and are not recorded.

At low incident angles, $\theta < (h/L)$ where h is the beam height and L is the length of the sample along the X-ray beam, the "footprint" of the X-ray beam on the sample is fixed and of magnitude L. Beyond this angle, the length of the footprint l decreases monotonically with θ. Specifically,

$$l = h/\theta \tag{4}$$

As a result, a smaller fraction of the film is illuminated by the X-ray beam as θ increases. A correction for this geometric effect was applied to the experimental data so that the fluorescence yield at each incident angle reported originates from a fixed sample area.

The distribution of zinc atoms in the organic film was determined by matching a theoretical model to the experimental data. Initially, a layered model of refractive index was used based on what was known about the structure of the sample. The Debye−Waller model[39] was used when the interfacial roughness was taken into account. A χ^2-fitting procedure[40] was used to fit the theoretical reflectivity derived from the Fresnel equations[30] to the experimental curve by adjusting the interfacial roughness value.[31,41] The interfacial roughness value yielding the best fit was used in the subsequent E-field intensity and fluorescence calculations. The multiple beam interference patterns observed in the reflectivity curve between 2.5 and 7.5 mrad (see below) were used to determine the total thickness of the organic film on top of the gold mirror.[29,34] This aspect of the data analysis will be addressed separately in the Results section.

The model distribution of zinc in the film normally consisted of a Gaussian distribution on a linear background with the latter accounting for a small fraction (<20%) of the total distribution. Introducing the linear background component improved the match between the calculation and the experimental fluorescence yield nodes at low angles (<3 mrad). The linear background is ascribed to defects introduced into the film during film deposition and/or an incoherent component in the X-ray E-field in the low-angle region. The mean position above the mirror surface and the half-width-at-half-height (hwhh) of the Gaussian were adjusted in the fitting protocol. The fits were executed interactively several times before using automatic iteration. The fluorescence data in the angular range of 3−8 mrad were most heavily weighted in the fitting procedures.[29]

We note that neither the E-field intensity distribution nor the fluorescence yield profile is particularly sensitive to the model distribution of optical indices in the organic films.[41] Thus, after a reasonable model is chosen for the sample at a certain temperature, an iterating correction of the model was not considered necessary and was omitted from the program. However, modifications to the refractive indices were always made when the film structure changed dramatically in the vicinity of the transition temperature since the air/film interface is no longer sharp. Above the transition temperature, the interface is described as a region with a continuously changing refractive index.[42]

Results

Thin Films. The angular dependence of the fluorescence and reflectivity data recorded at room temperature along with the theoretical fit for samples 1 and 4 are shown in Figure 3. The zinc distribution which gives the best fitting fluorescence yield curve is also included in Figure 3 along with the fitting parameters. The agreement between the experimental data and theory is remarkably good for both samples. As noted above, the position of the zinc layer can be derived qualitatively from the number of peaks appearing in the fluorescence yield profile at $\theta \leq \theta_c$. For example, in the case of sample 4 (with 16 bilayers of ωTA) 11 fluorescence peaks are observed in this region. The critical period, D_c, of the XSW in the organic thin film is 85 Å when X-ray refraction in the organic film is taken into account.[29] Thus, the zinc layer is located at approximately $(X - 0.5)D_c = 10.5D_c$ or 893 Å above the mirror surface. In the case of sample 1, the corresponding figure is $0.5D_c$ or 43 Å since a single complete peak is found in the fluorescence yield profile below θ_c. Both of these predicted values are consistent with the result obtained by careful curve fitting.

Well below the order−disorder transition temperature, the distribution of the zinc layer in the organic thin film in all the samples can be described accurately by a Gaussian distribution on a linear background with the latter accounting for a small fraction of the total distribution. An analysis of the fluorescence yield profiles obtained at room temperature indicates that the mean position of the zinc peak in samples 1−4 is 49, 165, 486, and 908 Å, respectively, above the gold mirror surface, with an associated hwhh ranging from 11 to 18 Å. Since the zinc atom layer distribution reported here is a one-dimensional projection onto the Z-axis along the mirror surface, the finite width of the Gaussian peaks reflects the roughness of the mirror surface and the nonuniformity of the organic films over the area of the sample intercepted by the X-ray beam footprint.

The reflectivity data in Figure 3C contain information regarding the surface roughness of the gold mirror and the total thickness of the deposited organic film. The surface roughness of the gold mirror was determined to be less than 3 Å when evaluated by the Debye−Waller model. The multiple beam interference pattern on the reflectivity curve below θ_c provides a direct measure of the thickness of the adlayer. From the modulations observed in the reflectivity curves of samples 2, 3, and 4, a total film thickness of 186, 505, 931 Å, respectively, with an estimated error of less than ±5 Å was determined. Unfortunately, however, the same analysis cannot be performed on sample 1 because this sample has an adlayer thickness which is sufficiently small that the interference effect is imperceptible (Figure 3A). Other details concerning the reflectivity and fluorescence curves have been described previously.[29,34]

Upon heating, the two types of samples used in this study, namely those with and without the intervening ωTA bilayers, behaved differently in terms of the transformations they underwent as reflected in the corresponding high-temperature zinc atom distribution. These thermotropic structural rearrangements are described below.

Samples 2, 3, and 4, were prepared with 2, 8, and 16 bilayers of ωTA, respectively, sandwiched between a lower ODT self-assembled monolayer (SAM) and an upper inverted ZnA bilayer. In all cases, sample structure is thermally stable up to 70 °C. For example, in the temperature range from RT to 70 °C, the

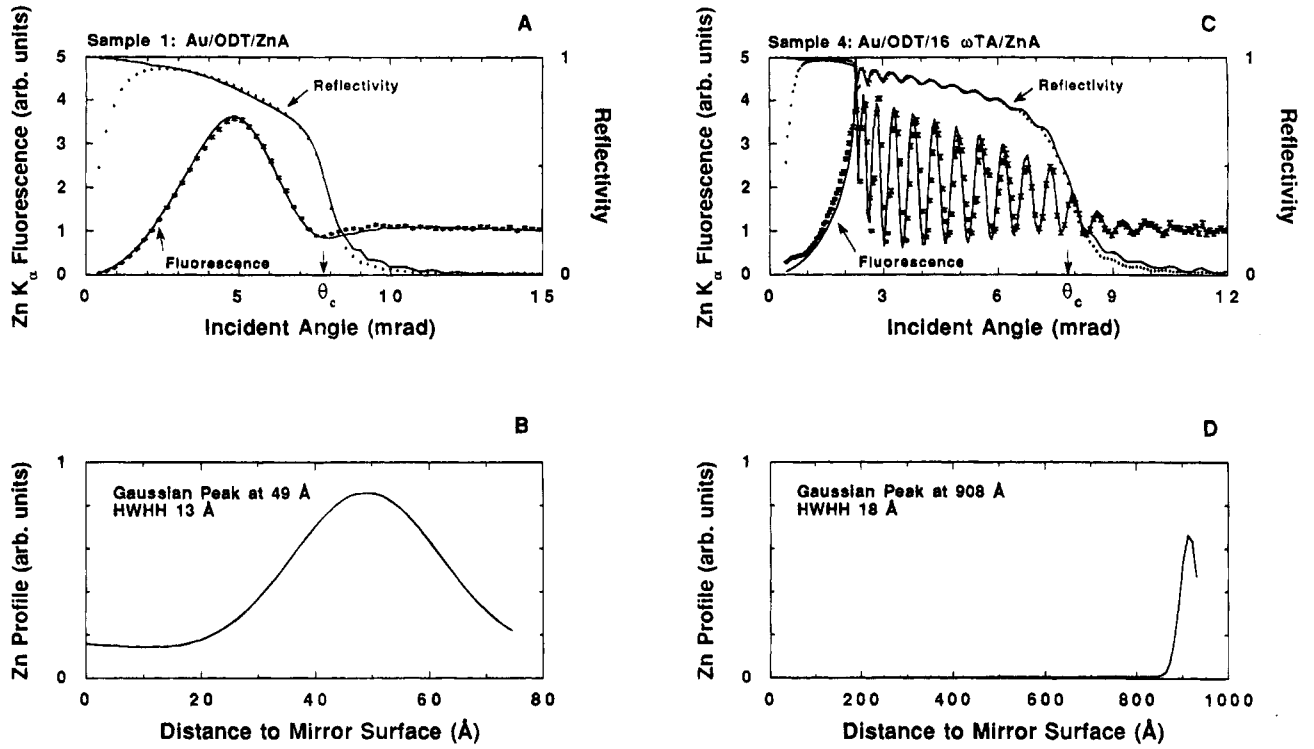

Figure 3. The experimental (circles) and theoretical (lines) angular dependence of the Zn Kα fluorescence yield and the specular reflectivity at 9.8 keV for samples 1 without (A) and with (C) ωTA bilayers. Sample composition is indicated at the top of each figure in the composite as appropriate, where "16 ωTA" is read 16 bilayers of ωTA. The same notation is used throughout the figures. The zinc distribution profiles above the mirror upon which the theoretical fluorescence yield profiles are based are shown in B and D. The fluorescence yields were normalized to the same area of illuminated film at all angles and scaled so that a fluorescence yield of unity is obtained beyond the critical angle. The critical angle of the gold mirror is 7.85 mrad and is indicated in the figure.

zinc layer position and the hwhh of the distribution in sample 2 fluctuates within a few angstroms (Figure 4 parts A and B). Since the magnitude of these fluctuations is comparable to the resolution of the measurement, viz., ca. 3 Å,[29] we interpret these data as indicating that there is no significant structural rearrangement occurring in the temperature range between RT and 70 °C. In samples containing a relatively large number (16) of ωTA bilayers, the zinc-to-mirror distance increases by more than 10 Å in this same temperature range (Figures 4 Parts C and D). However, there is no significant change in the hwhh of the zinc distribution associated with the thickness expansion of the film. In samples containing ωTA, when the temperature was increased by an additional 2 °C to 72 °C all modulations except for the first peak in the fluorescence yield profile decreased suddenly indicating that a major structural transformation had occurred in the film. This temperature is referred as the main transition temperature, T_m, of the thin film. T_m is close to but slightly below 72 °C. At T_m, an analysis of the fluorescence yield data suggests that the zinc layer has shifted closer to the mirror surface and that it has broadened considerably.

During the course of heating sample 2, the following two tests on the nature of the transition were performed. First, with an incubation temperature of 72 °C, the sample was translated 3 mm in the direction normal to the X-ray beam to examine a fresh strip of film. An identical fluorescence yield profile was obtained to that observed at the original exposure site at 72 °C. This demonstrated convincingly that the phase transition is due solely to thermal effects and is not an artifact of radiation damage. The second test consisted of a thermotropic reversibility study. Fluorescence and reflectivity data were recorded on a sample held at 72 °C and again when temperature was reduced to 68 °C and further to 63 °C with incubation time at each temperature of 30 min or more. The data indicate that the layered zinc distribution seen at low temperatures before passage through T_m was not restored upon sample cooling. Further, the hwhh remained in the vicinity of 100−130 Å upon cooling suggesting that in the case of sample 2 at least the thermotropic structural transformation is not reversible on the time scale of these measurements. This same observation holds true for all of the samples examined in the experiment.

At a temperature slightly above T_m, the zinc distribution in the organic film of all ωTA-containing samples is best described as a broad band (hwhh > 49 Å) whose center has shifted closer to the mirror surface compared to the distribution below T_m. Continued heating to well above T_m effected complete disordering of the film. The final high-temperature zinc distribution can be described as random throughout the adlayer (see the Discussion section).

In addition to the change seen in the fluorescence yield profiles, the reflectivity of the ωTA-containing samples also underwent a dramatic change in the same temperature range where the thermotropic transition, as evidenced by a change in the zinc distribution, occurred. Most obvious was the loss of interference modulations below θ_c at high temperature. This can be accounted for by (1) a roughening of the adlayer surface to such a degree that it no longer reflects the X-ray coherently and/or (2) a dramatic thinning of the film. The latter is unlikely the cause for the reflectivity change in our experiments since no desorption of the LB thin film material from the substrate is expected at these low temperatures nor was there a change in the total fluorescence yield (see the Discussion section). Therefore, a roughened air/organic film interface above T_m is assumed to be responsible for the loss of the modulations in the reflectivity curves seen below T_m. Accordingly, a new model for the refractive indices above T_m was used in the fitting protocol which assumes that the film has a continuously varying refractive index as a function of depth at the air/LB film

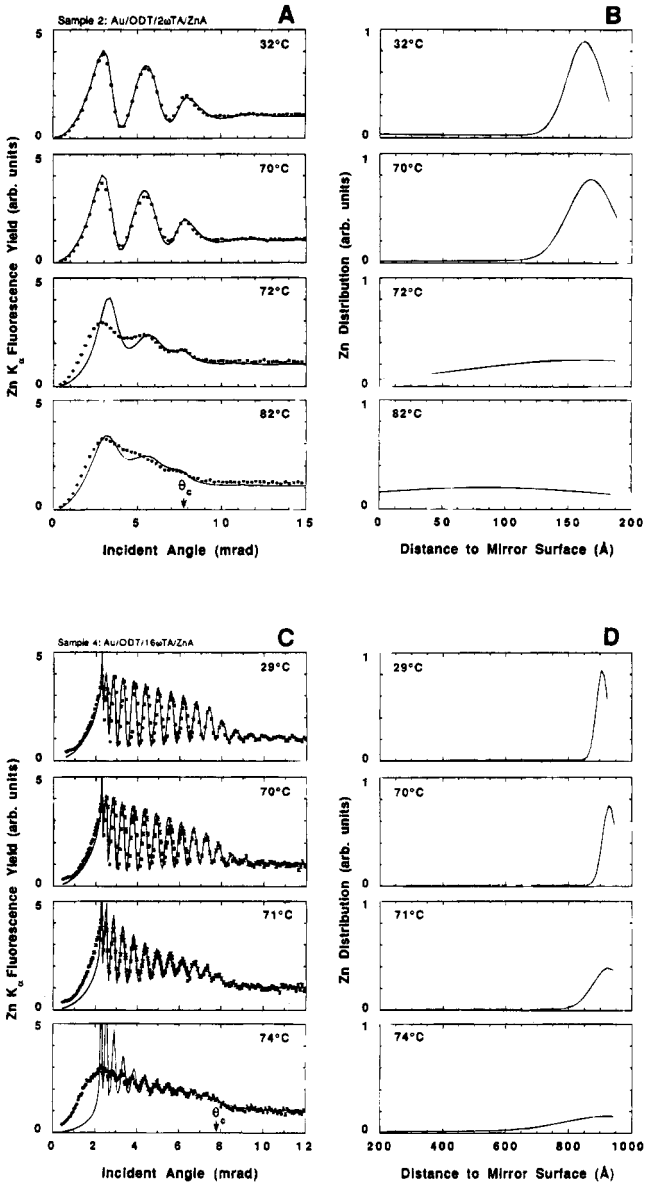

Figure 4. The experimental (circles) and theoretical (lines) angular dependence at 9.8 keV of the Zn Kα fluorescence yield for samples with 2 (A, sample 2) and 16 (C, sample 4) ωTA bilayers at the indicated temperatures. Experimental conditions and data manipulation are as described in the Methods section and in the legend to Figure 3. The calculated zinc distribution above the mirror surface is shown for samples with 2 (B) and 16 (D) ωTA bilayers.

interfacial region. The experimental data and theoretical fitting of the reflectivity of sample 2 above and below T_m are shown in Figure 5. The insects show the corresponding refractive index models used in fitting the reflectivity data.

The thermotropic properties of sample 1 prepared without ωTA and which had a single inverted bilayer of ZnA directly on top of the SAM of ODT were very different from those observed with the ωTA-containing samples (compare Figures 4 and 6). In the temperature range between 32 and 88 °C, the bulk of the zinc in sample 1 is located in a band centered ca. 45−49 Å above the mirror surface with a spread (hwhh) of 13−15 Å. Between 88 and 105 °C, the zinc layer began to broaden and to move toward the mirror surface indicating collapse of the film. At 105 °C, the mean position of the zinc layer above the mirror surface is 40 Å with a hwhh of 50 Å. Data collected at 91 °C on a fresh portion of the sample indicated that radiation damage was not a problem with sample 1. In the vicinity of 105 °C, the zinc atom distribution in the

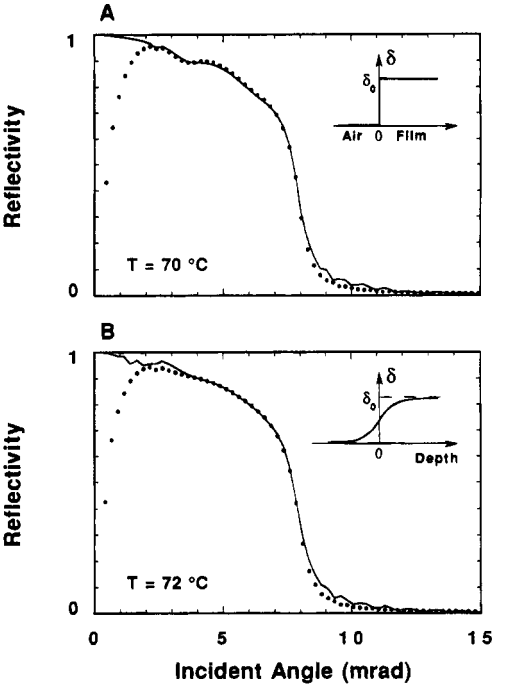

Figure 5. Measured (circles) and calculated (lines) reflectivity profiles for the sample incorporating 2 ωTA bilayers (sample 2) below (A) and above (B) the main transition temperature, T_m. Models of the refractive index profile used in the corresponding calculations are shown (not to scale) as insets in the figure. Below T_m, the air/film interface is assumed to be sharp (inset in A) and with the same surface roughness value (3 Å) found at the gold mirror surface. Above T_m, the modulations in the measured reflectivity curve disappear due to a roughening of the air/film interface (B). Accordingly, the interface is represented by a series of layers each 2 Å thick. The refractive index of each layer is set to the value determined by the refractive index model shown in the inset. The refractive index decrement of the organic thin film below T_m is δ_0 (= 2.5 × 10^{-6} at 9.8 keV).

film above the mirror surface can best be described as random. With continued heating, a second transition takes place in the sample at ca. 110 °C. This is characterized by an increase in the fluorescence counting rate in the vicinity of θ_c and a decrease in the fluorescence peak intensity at 5 mrad. Since the first antinode sites on the mirror surface at and above θ_c the fluorescence yield profile at 110 °C and above suggests that the zinc has migrated through the organic film and has formed a discrete condensed layer at the mirror surface. Such a model for the zinc distribution with a hwhh of 5 Å nicely matches the experimental fluorescence yield profile up to 129 °C with an increasing fraction of the zinc signal existing in the condensed layer at higher temperatures. Above 129 °C, the zinc fluorescence signal from the sample peaks just below θ_c at 7.5 mrad. A simple model to describe this unusual high-temperature fluorescence yield profile consisted of a concentrated layer of zinc at the mirror surface with a hwhh of 3 Å. The fluorescence yield profile observed at 129 °C persists upon cooling the sample to 32 °C and upon subsequent incubation at 32 °C for 15 h.

Bulk Materials. Thus far, we have shown that thin films containing ωTA undergo a thermally-induced transition at ca. 72 °C. This behavior is observed in samples with as few as two inverted bilayers of ωTA. In the measurements that follow, we wished to determine if the behavior of the ωTA in thin film form is reminiscent of that in bulk. This this end, we have performed SCALTRD measurements on dry ωTA powder (Figure 7).

The diffraction data are shown in the form of a streak film which amounts to a one-dimensional diffraction pattern recorded continuously as a function of time and thus, temperature, during

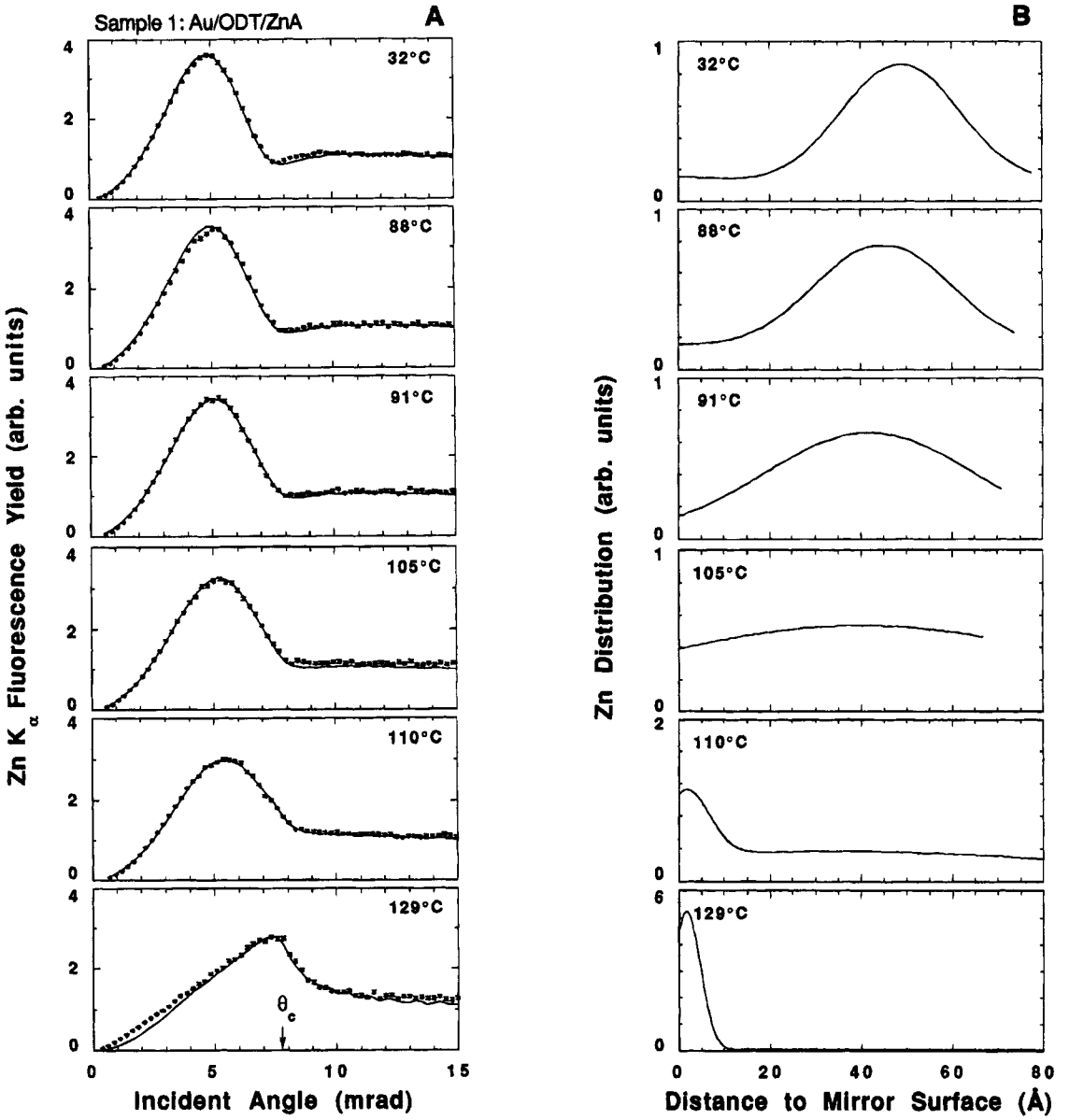

Figure 6. The experimental (circles) and theoretical (lines) angular dependence at 9.8 keV of the Zn Kα fluorescence yield (A) for sample 1 which lacks ωTA at the indicated temperatures. Experimental conditions and data manipulations are as described in the Methods section and in the legend to Figure 3. The calculated zinc distribution above the mirror surface is shown (B). The lamellar structure of the sample is stable up to ca. 88 °C, beyond which there are two different thermotropic events observed in the heating sequence. First, an order/disorder transition begins at 88 °C as evidence by the disappearance of the trough in the fluorescence yield profile in the vicinity of the critical angle (7.85 mrad). Above 110 °C, there is a significant reduction in the height of the fluorescence peak at ca. 5 mrad accompanied by the emergence of a peak just below θ_c indicating that the zinc migrates through the organic thin films and forms a condensed layer directly on top of the gold mirror surface.

the course of a simultaneous calorimetric heating scan performed on the same sample. In the low-angle region of the streak film a series of lamellar reflections with a repeat spacing of 49.9 Å is seen at low temperature (Figure 7). The wide-angle region is dominated by several sharp, as well as broad, reflections in the 3.6−4.3 Å range. Taken together, these data suggest that the ωTA at low temperature exists in the lamellar phase with the hydrocarbon portion of the fatty acid molecule in a crystalline-like packing arrangement. This is referred to as the lamellar crystalline (Lc) phase. The Lc phase persists up to ca. 70 °C with some slight rearrangement in the acyl chain packing taking place below 70 °C as evidenced by a broadening and a shifting about of certain of the wide-angle reflections in this temperature region. Complete melting to an isotropic fluid occurs at ca. 80 °C as evidenced by the disappearance of all sharp reflections in the pattern and the emergence of diffuse liquid-like scatter in both low- and wide-angle regions. These data suggest that ωTA does not exhibit thermotropic liquid crystal behavior, in the dry state at least, and that the transition seen between 70 and 80 °C represents a simple melting process.

The calorimetric behavior of the ωTA powder upon heating (from 60 to 90 °C) in the SCALTRD experiment shows a single large endotherm with an onset at ca. 70 °C and a maximum at 73.9 °C (Figure 7). The bulk of the transition as judged by calorimetry is complete by 75 °C. Cooling measurements in the SCALTRD apparatus show that the calorimetric transition has an onset temperature of 71.4 °C, a midpoint of 71 °C, and a final temperature of 70.2 °C. The onset of the recrystallization process as monitored by X-ray diffraction in this same experiment occurs at 70.5 °C (cooling data not shown).

The persistence of sharp reflections during heating in the streak film in the 75−80 °C range (Figure 7) beyond where the bulk of the calorimetric transition is registered is not fully understood. It is possible that the transition is indeed broad in

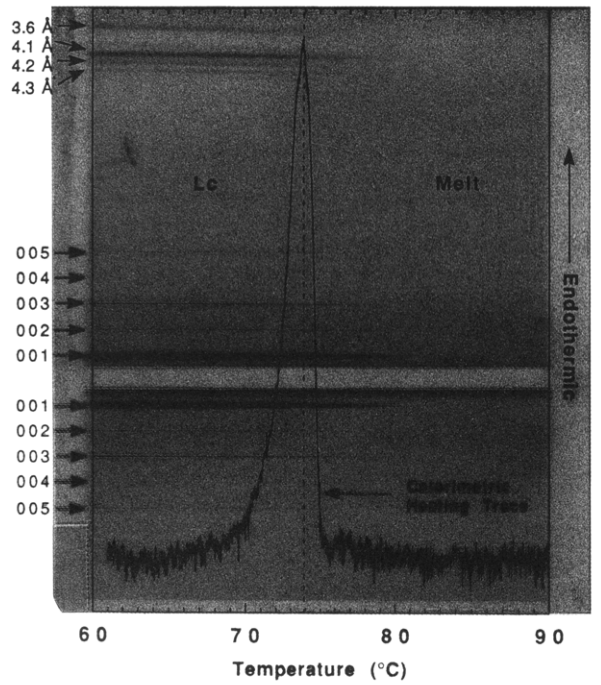

Figure 7. Simultaneous calorimetry and time-resolved X-ray diffraction measurements on dry powdered ωTA performed in the heating direction. Diffraction measurements were made with a streak camera as described in the Methods section. In the lamellar crystalline (Lc) phase, the low-angle reflections are indexed according to a lamellar lattice (d-spacing 49.9 Å) while the wide-angle reflections are labeled with their corresponding d-spacings. The calorimetric trace (marked) has been overlaid on the streak pattern. The vertical line indicates the endothermic peak temperature at 73.9 °C.

the 70−80 °C range and asymmetric with most of the melting occurring below 75 °C. Upon heating from 75 to 80 °C, the residual crystalline material melts, but because the amount of material involved is small, it contributes little to the calorimetric signal. In contrast, diffraction is profoundly sensitive to small amounts of a crystalline phase coexisting with a disordered phase[43] which, in this case, happens to be the melt. Thus, what may appear as a mismatch between the calorimetric and diffraction measurements in the SCALTRD study may simply reflect a differential sensitivity of the two methods to the phases involved.

In separate measurements performed using a high-sensitivity DSC (see the Methods section), essentially the same results as reported in Figure 7 were obtained. Here, the heating onset, peak maximum, and final temperatures were 70.5, 73.0, and 73.9 °C, respectively. The heating enthalpy of the transition was ca. 11.4 kcal/mol. In the cooling direction (rate 0.5 °C/min) the corresponding values are 70.5, 70.0, and 69.6 °C, respectively, with an enthalpy change of 11.7 kcal/mol.

Combining the simultaneous diffraction and calorimetry data, we can state that ωTA as a dry powder is stable in the Lc phase below 70 °C. In the temperature range 70−75 °C, the crystalline material undergoes a melting transition to an isotropic fluid. The transition is reversed upon cooling.

Discussion

To facilitate a discussion of the XSW fluorescence yield profile data presented in Figures 4 and 6, the thermotropic structural rearrangements occurring in samples 1−4 are summarized in Figure 8. In this plot, changes in the mean position of the zinc distribution in the LB film above the mirror surface and the associated hwhh are presented as a function of temperature in the heating direction.

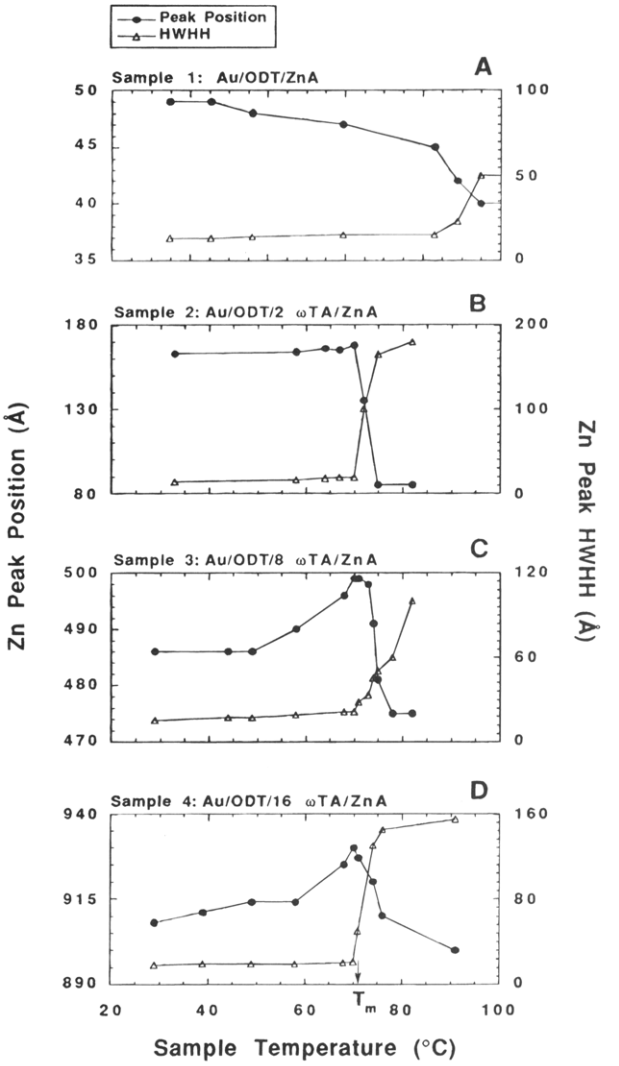

Figure 8. Temperature dependence of the position (filled circles) and width (open triangles) of the zinc layer above the mirror surface in a series of thin films incorporating a variable number of ωTA bilayers. Position and width refer to the peak and hwhh of the Gaussian that best describes zinc distribution above the mirror. Sample composition is indicated at the top of each figure in the composite. All measurements were made in the heating direction. The midpoint temperature of the transition, T_m, in the ωTA-containing samples in the vicinity of 72 °C is indicated.

In an effort to understand the relationship between the structure and the composition of paucilamellar LB films and their stability and thermotropic properties, the behavior of the two types of samples, namely, those with (samples 2−4) and without (sample 1) ωTA sandwiched between an upper ZnA inverted bilayer and a supporting SAM of ODT, will be compared.

Most notable about the thermotropic properties of sample 2, which incorporates two inverted bilayers of ωTA, is the sharpness of the transition between 70 and 72 °C. Indeed, it is possible that the transition is even more cooperative than indicated in this figure, the latter being limited by the 1−2 °C step sizes used to adjust sample temperature in the transition region. Below T_m in the range 32−70 °C, the film is structurally stable to within the sensitivity of this method (estimated at 3 Å) on the time scale of the measurements. A precipitous collapse of the film toward the substrate surface occurs in the transition temperature range. It is accompanied by a dramatic broadening of the zinc distribution.

Qualitatively, the same basic pattern of thermotropic behavior is seen with samples 3 and 4 which incorporate 8 and 16 ωTA

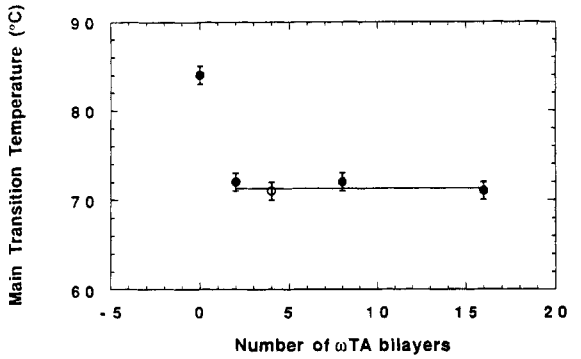

Figure 9. Dependence of the transition temperature determined by XSW on the number of ωTA bilayers in a composite organic thin film consisting of a lower SAM of ODT and an upper inverted bilayer of ZnA. Transition temperature data were obtained from Figure 8 and correspond to the temperature at which the hwhh of the zinc layer in the thin films increases dramatically. The transition temperature has an associated error of ± 1 °C due to the finite step size used in adjusting the sample temperature and the accuracy of the temperature controller and measuring devices. The horizontal line is drawn to guide the eye and to show the near constancy of the transition temperature with number of ωTA bilayers. A data point (open circle) has been included in this figure corresponding to a sample incorporating four ωTA bilayers. This sample was not described in the text because the LB films deposited on it were found to be structurally defective. This is evidenced by a much broader zinc distribution (hwhh > 40 Å) at room temperature as compared to the other samples. However, its T_m is very close to that found for the other ωTA-containing samples.

bilayers as was observed with sample 2. Below T_m, the zinc layer is narrow, well-defined, and relatively insensitive to temperature. Passage through T_m gives rise to a dramatic increase in the width of the zinc layer which coincides with a net movement of the zinc distribution center-of-mass toward the mirror surface. Unlike sample 2 where the zinc peak position remains constant to within the sensitivity of the measurement upon heating to just below T_m, in the case of samples 3 and 4 a slight but preceptible movement of this peak away from the mirror surface is seen. In both cases, the overall thickness expansion amounts to 3% in the temperature range from RT to 70 °C. Such a small fractional change in film thickness would not have been considered significant in the case of sample 2 with an overall thickness of 200 Å. The structural origin of the thickness expansion in samples 3 and 4 has not been determined but may relate to chain tilt angle.

Sample 1 posits an inverted bilayer of ZnA directly on top of the self-assembled ODT monolayer. Its thermotropic properties are quite in contrast to those observed with the others discussed above. To begin with, the temperature range where pronounced structural changes take place is shifted to higher temperatures. Further, the transition is not a simple transformation but occurs in a series of steps. The first involves a collapse of the zinc layer toward the mirror surface and a broadening of the zinc layer. This is followed by a complete disordering of the film where in the zinc is uniformly distributed throughout the film. As the temperature increases further the zinc moves to the surface of the mirror and assumes a condensed layer configuration presumably accompanied by a displacement of the ODT from the gold surface (*vide infra*).

The most significant difference in the behavior of the two types of LB films, namely those with and without ωTA, lies in the temperature and sharpness of the transition (Figure 8). In the ωTA samples, the transition is sharp, while it is broad in the sample without ωTA. The dependence of T_m on the number of ωTA bilayers in the composite films is plotted in Figure 9. Obviously, within the temperature resolution afforded by the current experimental arrangement, T_m is independent of the number of layers of ωTA down to as few as two bilayers. Further, it is quite distinct from that of the ωTA-free sample.

Our measurements on thin films indicate that the thermotropic transition seen between 70 and 72 °C which is independent of the number of ωTA layers present in the range 2−16 can be ascribed to the melting of the ωTA component. This statement is based on the observation that in the absence of ωTA, no transition is seen in the vicinity of 72 °C in the corresponding SAM/LB film. Further, ωTA in bulk form exhibits a reversible melting transition in the same temperature range. This is an important result since it illustrates that the melting transition characteristics of ωTA are preserved all the way from a bulk powder to a pair of inverted bilayer LB films sandwiched between a solid-supported SAM of ODT and an inverted bilayer LB overlayer of ZnA. The finding serves to emphasize the strength of the lateral intermolecular forces in ωTA and the relative insensitivity of the film to surface and dimensionality effects.

While the melting characteristics are similar, what distinguishes the behavior of ωTA in thin film form from that in bulk form is reversibility. The melting transition is thermally reversible in the bulk material but irreversible, on the time scale of these experiments, in the thin film form. LB films of polymer material have been shown to undergo reversible thermal transitions[44,45] based on X-ray diffraction and infrared spectroscopy measurements. It is likely, however, that in the case of the ωTA-containing samples which are not polymeric, the irreversible melting reflects the complex nature of the films involved which consist of three different types of materials organized as SAMs or LB films. Thus, when the ωTA film melts, the highly stratified and ordered nature of the original composite film is lost and mixing of components from the different strata occurs. Simply by cooling, the mixing cannot be undone and the original segregated lamellarity restored. The situation is quite different in the case of the ωTA powder. Here, the phase change represents a transition between crystalline order and liquid disorder. By lowering the temperature through the melting point, the original crystalline order is thermodynamically favored and easily accessed. Because the material is pure to begin with, the transition does not involve a mixing/demixing of components.

While the description of the zinc distribution in the ωTA-containing samples used in this study as being Gaussian and of finite width below T_m is reliable, we are less confident in our appraisal of its distribution at higher temperatures. This is apparent when the mismatch between the experimental and calculated fluorescence yield profiles in Figures 4 and 6 is considered. Certainly, at high temperatures, the zinc distribution broadens considerably compared to that at low temperatures. This is reflected in the reduced modulation amplitude in the corresponding fluorescence yield profile. However, the mismatch is such that a single broad Gaussian distribution does not account for all of the zinc present in the film. Further, a completely random distribution model does not fit the data well even at the highest temperatures studied, above 100 °C. Thus, we speculate that at high temperatures, where the ωTA has melted, the ZnA phase separates and exists as isolated domains or patches of ZnA pauci- or multilayers on the mirror or SAM surface. This finding agrees with the droplet model of Tippmann−Krayer *et al.*[46] for the final high-temperature state of a sample which started out as a ZnA LB film at low temperatures. In their model, zinc ions condense into isolated droplets suspended in the ZnA thin film while the sample is well above the film melting temperature. In related studies using only CdA and ZnA LB films, the high-temperature configuration appeared

to remain ordered while at the same time having undergone significant thinning.[20,21]

In the case of sample 1 which lacks ωTA and which has a ZnA inverted bilayer positioned directly on top of the SAM of ODT, a very different thermotropic behavior was observed (Figure 8A). In contrast to the ωTA-containing films, sample 1 underwent a dramatic structural rearrangement some 20 °C above that recorded for samples 2−4. Preceding the transition, there is a gradual thinning of the film by 4−5 Å in the range 25−88 °C. In this interval, the hwhh of the zinc layer remains relatively constant. This is followed by a sudden shift in the position of the zinc layer toward the mirror surface by ca. 5 Å over a 10 °C interval beginning at 88 °C. Concomitantly, the hwhh of the zinc layer more than triples. Qualitatively, these data are not unlike those reported previously for a CdA/ZnA LB film.[20] With continued heating above this initial low-temperature transition, which moves the zinc layer toward the mirror surface, there is an additional structural rearrangement that causes the zinc to relocate and to position itself directly at the mirror surface. This is particularly evident at temperatures above 129 °C where the zinc fluorescence peaks in the yield profile just below θ_c (Figure 6). For such a dramatic change to occur, however, it is necessary that the SAM of ODT be displaced from the mirror surface. This observation is consistent with the behavior of ODT monolayers on Au(111) investigated by Fenter *et al.*[47]

At incident angles beyond θ_c, the X-ray beam is minimally reflected from the mirror surface. The net effect is for the intensity modulation in the XSW to fall off dramatically in this angular range. Thus, any X-ray fluorescence from the sample beyond θ_c is a measure of the total number of heavy atoms in the thin film above the mirror intercepted by the incident X-ray beam. With all the samples used in this study, the Zn Kα fluorescence yield beyond θ_c remained constant as a function of temperature. This indicates that the total amount of zinc in the film remained fixed and that no zinc escaped from the sample even up to 140 °C, the highest temperature used in this study.

An important control experiment was included in this study which addresses the issue of radiation damage. By translating the sample in the X-ray beam to expose a fresh part of the film, it was shown that under the conditions of these measurements and for all of the samples, radiation effects were not important. Parenthetically, we note that radiation damage can be limiting not only with thin films of the type used in these experiments (unpublished data) but also with hydrated bulk lipid samples.[48,49]

Conclusion

A variable period XSW generated by total external reflection from a gold mirror has been used in an element-specific manner to monitor directly the thermally-induced structural changes occurring in paucilamellar LB films containing an inverted bilayer of ZnA which served as an indicator of thin film structural integrity. The zinc distribution in the film was determined with angstrom resolution by fitting the experimental angle-dependent X-ray fluorescence data to a theoretical model. The data show that gold mirror-supported films incorporating ωTA are structurally stable up to 70 °C beyond which an irreversible change takes place which involves a dramatic relocation of the zinc above the mirror surface. The transition reflects the melting in the ωTA component of the composite film. Given that the transition coincides with the melting temperature of ωTA in bulk form, the remarkable result emerges that bulk thermal behavior is preserved all the way down to as few as two bilayers with the latter sandwiched between an SAM and an LB bilayer. In addition to highlighting the strength of intermolecular interactions that exist in ωTA-containing films this study has demonstrated convincingly that the XSW and reflectivity measurements permit sensitive and detailed mensuration of paucilamellar films and their components. The success of these measurements indicates that the variable period XSW method might now be used to study membrane lipid and protein topology and to obtain heavy atom position information not only in membranes but also in peripheral components such as membrane-associated antibodies and cytoskeletal and peripheral proteins.

Acknowledgment. The help and support of the entire CHESS (National Science Foundation Grant DMR 12822) staff and G. Navrotski, in particular, are acknowledged. Many thanks go to G. M. Bommarito for invaluable advice regarding both theoretical and experimental aspects of this work. We are grateful to J. Briggs for making possible and participating in the SCALTRD measurements. We also thank Z. Yin and X. Huang for helping with sample preparation and data analysis and H. Chung and A. Cheng for assistance with the X-ray diffraction and calorimetry measurements. This work was supported by grants from the National Institutes of Health (DK 36849 and DK 45295) and the National Science Foundation (DIR-9016683) to M.C. and by DOE (W-31-109-ENG-38) to ANL for M.J.B.

References and Notes

(1) Roberts, G. G. In *Langmuir-Blodgett Films*, 1st ed.; Roberts, G. G., Ed.; Plenum Press: New York, 1990; p 317.
(2) Roberts, G. G. *Contemp. Phys.* **1984**, *25*, 109.
(3) Zasadzinski, J. A.; Viswanathan, R.; Madsen, L.; Garnaes, J.; Schwartz, D. K. *Science* **1994**, *263*, 1726.
(4) Bonnerot, A.; Chollet, P. C.; Frisby, H.; Hoclet, M. *J. Chem. Phys.* **1985**, *97*, 365.
(5) Käs, J.; Sachmann, E. *Biophys. J.* **1991**, *60*, 825.
(6) Buhaenko, M. R.; Grundy, M. J.; Richardson, R. M.; Roser, S. J. *Thin Solid Films* **1988**, *159*, 253.
(7) Prakach, M.; Ketterson, J. B.; Dutta, P. *Thin Solid Films* **1985**, *134*, 1.
(8) Penfold, J.; Thomas, K. R. *J. Phys.: Condens. Matter* **1990**, *2*, 1369.
(9) Nicklow, R. M.; Pomeranty, M.; Segmüller, A. *Phys. Rev. B* **1981**, *23*, 1081.
(10) Riegler, H. E. *J. Phys. Chem.* **1989**, *93*, 6475.
(11) Drexhage, K. H. In *Progress in Optics*; Wolf, E., Ed.; North-Holland: Amsterdam, 1974; Vol. XII; p 165.
(12) Rabolt, J. F.; Burns, F. C.; Schlotter, N.; Swanlen, J. D. *J. Chem. Phys.* **1983**, *78*, 964.
(13) Kimura, F.; Umemura, J.; Takenaka, T. *Langmuir* **1986**, *2*, 96.
(14) Golden, W. G.; Snyder, C. D.; Smith, B. *J. Phys. Chem.* **1982**, *86*, 4675.
(15) Dierker, S. B.; Murray, C. A.; Legrange, J. D.; Schlotter, N. E. *Chem. Phys. Lett.* **1987**, *137*, 453.
(16) Kobayaoshi, K.; Takanaka, K.; Ochiai, S. *Thin Solid Films* **1988**, *159*, 267.
(17) Laxhuber, L.; Möhwald, H.; Hashmi, M. *Int. J. Mass Spectrom. Ion Phys.* **1983**, *51*, 93.
(18) Schwartz, D. K.; Gernaes, J.; Riswanathan, R.; Zasadzinski, J. A. N. *Science* **1992**, *257*, 508.
(19) Iida, A.; Matsushita, T.; Ishikawa, T. *Jpn. J. Appl. Phys.* **1985**, *24*, L675.
(20) Bedzyk, M. J.; Bilderback, D. H.; Bommarito, G. M.; Caffrey, M.; Shildkraut, J. *Science* **1988**, *241*, 1788.
(21) Bedzyk, M. J.; Bommarito, G. M.; Shildkraut, J. *Phys. Rev. Lett.* **1989**, 1376.
(22) Zheludeva, S. I.; Lagomarsino, S.; Novikova, N. N.; Kovalchuk, M. V.; Scarinci, F. *Thin Solid Films* **1990**, *193/194*, 395.
(23) Batterman, B. W. *Phys. Rev.* **1964**, *133*, A759.
(24) Batterman, B. W. *Phys. Rev. Lett.* **1969**, *22*, 703.
(25) Anderson, S. K.; Golovchenko, J. A.; Mair, G. *Phys. Rev. Lett.* **1976**, *37*, 1141.
(26) Cowan, P. L.; Golovchenko, J. A.; Robinsons, M. F. *Phys. Rev. Lett.* **1982**, *44*, 1680.
(27) Golovchenko, J. A.; Patel, J. R.; Kaplan, D. R.; Cowan, P. L.; Bedzyk, M. J. *Phys. Rev. Lett.* **1982**, *49*, 560.

(28) Bedzyk, M. J.; Materlik, G. *Phys. Rev. B* **1985**, *31*, 4110.
(29) Wang, J.; Bedzyk, M. J.; Penner, T.; Caffrey, M. *Nature* **1991**, *254*, 377.
(30) Parratt, L. G. *Phys. Rev.* **1954**, *95*, 359.
(31) Bommarito, G. M. M.S. Thesis, Cornell University, 1987.
(32) Ulman, A. *Ultrathin Organic Films*; Academic Press: San Diego, 1991.
(33) We measured an LB film sample whose structure is identical to that of sample 2 (Au/ODT/2ωTA/ZnA) by means of the X-ray standing wave technique immediately after the sample was prepared and some 3 years hence. The zinc Kα fluorescence yield profiles from the two measurements are identical (data not shown).
(34) Wang, J.; Bedzyk, M. J.; Caffrey, M. *Science* **1992**, *258*, 775.
(35) Chung, H.; Caffrey, M. *Biophys. J.* **1992**, *63*, 438.
(36) Briggs, J.; Caffrey, M. Manuscript in preparation.
(37) Zhu, T.; Caffrey, M. *Biophys. J.* **1993**, *65*, 939.
(38) Briggs, J.; Caffrey, M. *Biophys. J.* **1994**, *66*, 573.
(39) de Boer, D. K. G. *Phys. Rev. B* **1991**, *44*, 498.
(40) Press, W. H.; Flannery, B. P.; Teukolsky, S. A.; Vetterling, W. T. *Numerical Rescipes*, 1st ed.; Cambridge University Press: London, 1987.
(41) Wang, J. Ph.D. Thesis, The Ohio State University, Columbus, OH, 1994.
(42) Névot, L.; Groce, P. *Rev. Phys. Appl.* **1980**, *15*, 761.
(43) Caffrey, M.; Feigenson, G. W. *Biochemistry* **1984**, *23*, 323.
(44) Biddle, M. B.; Lando, J. B.; Ringsdorf, H.; Schmidt, G.; Schneider, J. *Colloid Polym. Sci.* **1988**, *266*, 806.
(45) Schneider, J.; Ringsdorf, H.; Rabolt, J. F. *Macromolecules* **1989**, *22*, 205.
(46) Tippmann-Krayer, P.; Mohwald, H.; L'vov, Y. M. *Langmuir* **1991**, *7*, 2298.
(47) With ODT, partial desorbtion from Au(111) was observed after incubating the sample for several hours at 120 °C. This was preceded by a solid-to-fluid transition (as defined in Fenter, P.; Eisenberger, P.; Liang, K. S. *Phys. Rev. Lett.* **1994**, *70*, 2447) starting at ca. 110 °C (P. Fenter, personal communication).
(48) Caffrey, M. *Nucl. Instrum. Methods* **1984**, *222*, 329.
(49) Cheng, A.-C.; Hogan, J. L.; Caffrey, M. *J. Mol. Biol.* **1993**, *229*, 291.